Surface Science 134 (1983) 499–528
North-Holland Publishing Company

A LEELS AND AUGER STUDY OF THE OXIDATION OF LIQUID AND SOLID TIN

A.J. BEVOLO, J.D. VERHOEVEN and M. NOACK

*Ames Laboratory–USDOE *, Iowa State University, Ames, Iowa 50011, USA*

Received 15 April 1983

The oxidation of liquid and solid tin from 25 to 240°C has been investigated using 75 eV low energy electron loss spectroscopy (LEELS) and Auger spectroscopy over an oxygen exposure range from zero to 10^7 L. LEELS was chosen for two reasons. First it can distinguish Sn, SnO and SnO_2 from each other. Second, we show that at 75 eV incident energy LEELS has a penetration depth of only one monolayer. As a result the continuity and stoichiometry of the oxide layer could be studied as a function of thickness from submonolayer to several monolayer thicknesses. Although unable to distinguish SnO from SnO_2 the larger penetration depth of the Auger technique complemented the LEELS study. From zero to one monolayer the oxide grows as islands containing both SnO and SnO_2. Above one monolayer coverage the oxide is continuous and free of metallic tin with its outer most surface enriched in SnO_2. Although oxide films grew more rapidly on polycrystalline tin than on single crystal tin the composition and continuity as a function of thickness remained unchanged. Very little change in oxide growth rate, continuity, or stoichiometry was observed for solid tin up to temperatures near the melting point. However at 229°C, just 3°C below the melting point of tin, dissolution of oxygen into the metal was observed. A continuous, metal free solid oxide, primarily SnO, could be grown on liquid tin at 240°C than remained stable for 20 min after removal of the oxygen gas. Our model for the early stages of the oxidation of tin is different from that previously proposed on the basis of UPS, XPS, and 400 eV LEELS with respect to the continuity and relative ordering of the SnO and SnO_2 phases. Quantitative comparison of our results with those previously reported shows that the previous results are consistent with our model for the structure and stoichiometry of the initial oxide grown on tin.

1. Introduction

Various types of convection can be sources of inhomogeneous distribution of dopants in float zone refined silicon. These defects become more important as the size of circuit elements is reduced. Surface tension driven convection (Marangoni convection) belongs to the class of convective flow that is indepen-

* Operated for the USDOE by Iowa State University under contract No. W-7405-Eng-82. This work was supported by the Director for Energy Research, Office of Basic Energy Sciences, WPAS-KC-02-01-02.

0039-6028/83/0000–0000/$03.00 © 1983 North-Holland

dent of gravitational forces and therefore would be present and perhaps dominant in the microgravity environment of the space shuttle. It may be possible to suppress Marangoni convection in the liquid phase by a thin oxide film. If this oxide film is continuous and has sufficient strength to support shear stress at the oxide/liquid interface, then the no slip condition should suppress Marangoni convection. The strength of the oxide film depends on its thickness and composition. An oxide film only a few monolayers thick may be sufficient if the film is continuous as opposed to an island structure. Classical techniques such as weight gain after oxidation are not sensitive enough to detect such thin films and do not give direct information on composition. However, surface analytical techniques such as photoemission (PES) and Auger (AES) spectroscopies are ideally suited to the study of thin oxide films. These techniques, because of their surface sensitivity, require ultra high vacuum compatible liquid samples, in particular those that have very low vapor pressures in the liquid state. Unfortunately silicon does not satisfy these requirements. Instead we have chosen tin to study the effects of oxide films on Marangoni convection and here we report on some characteristics of the oxides formed on molten tin.

Tin has two oxide phases, SnO and SnO_2. As a result the surface analytical technique must be able to distinguish SnO and SnO_2 from each other as well as metallic tin to determine stoichiometry. The most commonly used chemically sensitive surface techniques is PES. Core level bonding energies of the 3d state using X-ray PES (XPS) have shown [1,2] that metallic tin can be readily distinguished from either oxide phase by the 1.65 eV shift of this transition upon oxidation. No reliable chemical shifts have been observed in core level XPS between SnO and SnO_2. However, such shifts have been reported between SnO and SnO_2 using valence band photoemission studies (both UPS [3,4] and XPS [2]). The changes in the valence band spectrum of Sn, SnO and SnO_2 are sufficient to detect any of the phases in the presence of the other two. The knowledge of the stoichiometry versus depth of the oxide layer on tin requires the use of ion beam sputtering, which is awkward to perform in most photoemission spectrometers. As a result valence band PES was not used in this study.

All previous [4–7] AES studies have shown that metallic tin can be readily distinguished from either oxide phase. However, there is disagreement in the literature on whether the two oxide phases can be distinguished by AES. Our results (see below) confirm those of Powell [4] and not those of Sen et al. [6] that the Auger spectrum of the two oxide phases of tin are nearly identical and cannot be used, even qualitatively, to determine the relative fraction of either oxide phase in the presence of the other.

Powell [4] has shown, using UPS to verify the presence of SnO of SnO_2 on the surface, that low energy electron loss spectroscopy (LEELS) can distinguish all three tin phases by virtue of the differences in the energies of the bulk and

surface plasmon from the various phases. LEELS has been chosen to study the oxidation of tin over a temperature range that includes liquid tin for the following reasons. First, LEELS can be made very surface sensitive by adjusting the incident electron beam energy to take advantage of the minimum in the inelastic mean free path that occurs near 100 eV [8]. Second, surface plasmons observed in LEELS, which are confined to the top monolayer of the sample, provide enhanced surface sensitivity. Studies such as those of Namba et al. [9] on the oxidation of single crystal Mg illustrate the surface sensitivity of LEELS. In contrast to the atomically localized excitation of PES, AES and even ionization losses observed in LEELS, surface plasmons are spatially extended in the plane of the sample surface. As a result surface plasmons can readily distinguish correlated or island growth from uniform oxide layer growth at oxygen coverages of less than one monolayer. For island type oxide growth surface plasmons from the oxide and metal phases will be present simultaneously and two surface plasmons with different energies will be observed. For uniform growth there will be one surface plasmon whose energy continuously shifts with oxygen coverage. Both types of behavior have been previously reported [9,10]. Third, as we show below in the case of tin, the $4d_{3/2}$ and $4d_{5/2}$ core levels can be observed as ionization loss peaks with good intensity relative to the plasmon peaks. Finally LEELS can be performed without additional components using the same spectrometer required for AES. There are some disadvantages of LEELS as we have used it in this study. Our combined LEELS–AES spectrometer has a low energy resolution of about 0.6 to 1.0%. As a result we cannot observe vibrational energy losses. Also the plasmon peaks occur over a 20 eV energy range and the overlap of the plasmon peaks from the various tin phases becomes an important limitation.

The recent study of the oxidation of evaporated tin films by Sen et al. [7] used XPS and AES but did not attempt to distinguish SnO from SnO_2 in the oxide films. They did however confirm the enhanced surface sensitivity of surface plasmon losses in the tin 4d XPS spectrum versus that of the bulk plasmon losses. Oxidation studies of solid tin, capable of distinguishing SnO from SnO_2, have been performed by Lau and Wertheim [2] using valence band XPS and by Powell [4] using valence band UPS and LEELS. Both of these studies used evaporated tin films with oxygen exposures up to 10^6 L. Lau and Wertheim [2] found both oxide phases in the oxide layer after high oxygen exposures as well as metallic tin but did not propose any ordering of the various tin phases with respect to depth. Powell [4] also observed all three tin phases at high oxygen exposures using UPS but only SnO and Sn using LEELS. He proposed that SnO_2 was formed below SnO which was adjacent to the pure tin substrate and that both phases were permeated with metallic tin in the oxide film. Part of the evidence for this unusual ordering of the two oxide phases can from Powell and Spicer [3] who observed that the workfunction of tin changed very little for oxygen exposures up to 10^4 L. This they ascribed to

the continued presence of metallic tin observed in UPS spectra. Neither Lau [2] nor Powell [4] considered the possibility of island oxide growth which would account for the continued presence of metallic tin peaks observed in the various surface sensitive spectroscopies used previously and the workfunction results. Also the effects of the finite sampling depth of the techniques was not quantitatively considered. Powell [4] suggested that it might be possible that a continuous, fully oxidized layer containing only SnO or SnO_2 or both could still produce metallic tin signals from the underlying metallic tin phase. However, he preferred the mixed Sn, SnO and SnO_2 oxide layer model.

The inelastic mean free path of the electrons detected by AES, XPS, and 400 eV LEELS used by Lau [2] and Powell [4] have a value of about 15 Å or more [8]. It would appear (see below for quantitative confirmation) that a continuous oxide film even 10 Å thick, but free of metallic tin, could exist and yet metallic tin signals from the underlying metal substrate would form a significant fraction of the spectra acquired by these techniques. To detect the continuity of metal free oxide films of the order of 2 to 4 monolayers thick (5 to 10 Å) requires a penetration depth of almost one monolayer, or about 2.5 Å. Because of the strong attenuation of the 75 eV electron beam used in our LEELS study both into and out of the sample and the non-normal incidence angle of the electron beam, we show below that this leads to a penetration depth of nearly one monolayer for 75 eV LEELS. Although our principal interest originally was the study of the oxide film on liquid tin we have taken advantage of the extreme surface sensitivity of 75 eV LEELS to investigate the oxidation of solid tin as well. To our knowledge there has been no previous surface analytical studies of the oxidation of liquid tin.

It is the purpose of this work to use 75 eV LEELS and AES to study the oxidation of tin from 25 to 240°C (both solid and liquid phases) over an oxygen exposure range from 0 to 10^7 L. The aim was to discover under what conditions, if any, a metal free oxide layer exists and becomes continuous and to determine the thickness and stoichiometry versus depth of the oxide layer on tin. At low oxygen exposures simultaneous oxygen dosing and LEELS measurements were made to monitor the continuity and surface composition of the oxide layer during the initial stages of oxide growth. Ion beam depth profiles, using LEELS and AES, were performed to determine the relative concentration of all three tin phases with depth in a manner previously reported by us [11] for the native oxide of tin. These depth profiles were also used to determine the thickness of the oxide layer.

2. Experimental

The combined LEELS and AES spectrometer consisted of a Model 10-155 Physical Electronics cylindrical mirror analyzer with a coaxial electron gun. By

adjusting the electron gun controls, a 2.5 μA, 75 eV beam with a spot size of 250 μm could be generated for LEELS and a 1.0 μA, 3 keV beam with a spot size of 35 μm could be generated for AES. All LEELS spectra were acquired in the first derivative mode with a 0.25 eV modulation amplitude using lock-in detection with a time constant of 0.03 s. No effects due to electron beam heating or beam induced absorption or desorption were evident under the conditions of our experiments. An Ar^+ ion beam with an energy of 1.0 keV was used to clean the tin samples and generate the depth profiles. Unless otherwise stated, the depth profiles were carried out with the ion beam rastered over a 5×8 mm^2 area using an ion current of 100 nA. The ion beam intersected the horizontal electron beam at an angle of 72° at the sample surface in the vertical plane.

Three types of tin samples were investigated. Polycrystalline cast tin coupons, electropolished in 6% perchloric acid methanol solution at −60°C, were measured in the solid state at temperatures of 25, 100, 200, 220 and 229°C. These samples had their surface normals at angles θ_i of 0°, 45° or 60° with respect to the electron beam. A single crystal disk of tin was investigated at 200°C with $\theta_i = 45°$. Finally, a remelted, smooth tin ball was investigated in both the liquid (240°C) and solid (200°C) phases with $\theta_i = 45°$. All samples measured above room temperature were heated indirectly and their temperatures were measured with a thermocouple in direct contact with the sample.

The base pressure in the vacuum chamber during LEELS and AES measurements prior to oxygen exposure was 1×10^{-10} Torr. Residual gases were monitored by a UTI 100C quadrupole RGA with iridium filaments that permitted measurements of the background gases with oxygen pressures in the range from 2×10^{-8} to 5×10^{-4} Torr. In all cases the molecular oxygen 32 peak was at least two orders of magnitude greater than that of any other except the atomic oxygen 16 peak which was approximately 10 times smaller than the oxygen 36 peak. Hydrogen at mass 2 was a peak about 1/5 that of the 32 peak. To achieve these low levels of background gas a continuous flow of oxygen was necessary. At oxygen pressures in the 10^{-8} Torr region the Ti sublimation pump and a 400 l/s ion pump remained on and a poppet valve between the pumps and the analysis chamber was left fully open. At oxygen pressures near 10^{-4} Torr region both pumps were left on but the poppet valve was kept nearly closed to accommodate the large pressure differential between the pumps ($\sim 10^{-7}$ Torr) and the sample ($\sim 10^{-4}$ Torr).

A typical oxygen exposure experiment was performed in the following manner. After reaching its base pressure, with the sample stabilized at the desired temperature and the electron and ion gun filaments on, the vacuum chamber was backfilled with argon gas to a pressure of 7×10^{-5} Torr. The ion gun was then used to bombard the sample until LEELS signals characteristic of only metallic tin were observed. After an additional ion etching time of about 10 min the argon gas was removed by the ion pump and the ion gun was

turned off. Within 5 min the pressure in the vacuum chamber was in the 10^{-10} Torr region. Special care was required to insure the cleanliness of the smooth tin ball that was to be used in the liquid state. Before melting, the complete sample was ion etched until the portion analyzed by the electron gun was determined to be clean. Because of the orientation of the ion beam, approximately one-fourth of the ball could not be ion etched. After melting, contamination became evident presumably due to the migration of the unsputtered native oxide across the cleaned portion of the ball. The ion gun was again turned on and eventually the molten tin surface would remain free of contaminants even after the ion beam was removed. To prevent reaction with the molten tin, the container was made of oxidized tantalum. A stainless steel container proved unsatisfactory because of chrome oxide contamination. After the cleanliness of the sample surface was established, oxygen was introduced into the chamber and its pressure was stabilized by adjusting the oxygen flow rate and the poppet valve opening. In an oxygen pressure range of 10^{-8} Torr LEELS or AES spectra could be obtained in the presence of the oxygen without apparent damage to the electron gun filament. This was not possible for oxygen partial pressures in the 10^{-4} Torr range. In this case LEELS and AES spectra were recorded only after the oxygen was evacuated. The time delay between the removal of the oxygen and the acquisition of the spectrum was usually less than 1 min.

A check was made on the effects of the residual gases (H_2, H_2O, CO) at the 10^{-10} Torr range on the LEELS spectra. Prior to the introduction of oxygen the sputter cleaned surface was monitored for period of time equal to the longest oxygen exposures used. During the first 40 min no changes were found in the LEELS spectrum. After this period small changes were observed that indicated a very low level of contamination of the surface had occurred. These changes were smaller than those observed after an oxygen exposure of only 2 L which was usually accomplished in less than 1 min exposure. As a result we were confident that the residual gases were not significantly affecting our results during oxygen exposure.

3. Results

3.1. Background

There were several important considerations in our choice of 75 eV incident electrons used in LEELS rather than the 400 eV LEELS used by Powell [4]. Based on the inelastic mean free path versus energy as compiled by Seah and Dench [8], a value of 7.6 Å is expected at 75 eV compared to that of 15.6 Å at 400 eV for inorganic solids, i.e. SnO and SnO_2 in our case. We show below that this leads to a significantly better surface sensitivity at 75 eV compared to that

at 400 eV. This increased surface sensitivity was vital in our studies of the continuity of the oxide film at very low coverages. The energy width of the elastic peak was 0.7 eV at 75 eV compared to 1.8 eV at 400 eV, which was important for our requirement to resolve all six plasmons, two each from Sn, SnO and SnO_2. The $4d_{3/2,5/2}$ ionization loss doublet of tin is more intense and better resolved at 75 eV than at 400 eV. These differences are illustrated in fig. 1 where the LEELS spectra of clean tin is given for 75 and 400 eV incident

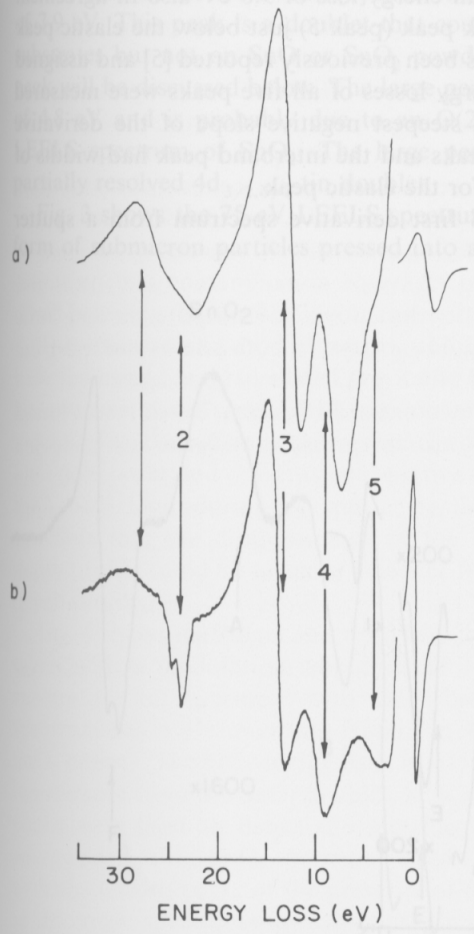

Fig. 1. Comparison of the first derivative LEELS spectrum of pure tin taken with an incident electron energy of 400 eV (a) and 75 eV (b). The peak at 0 eV loss is the elastic peak. Peak 1 is a double bulk plasmon loss at 28 eV. Peak 2 is the $4d_{3/2}$, $4d_{5/2}$ core level ionization loss of tin. Peak 3 is the bulk plasmon loss. Peak 4 is the surface plasmon loss and peak 5 is an interband transition. The 75 LEELS spectrum shows a more intense and better resolved 4d tin doublet and interband transition.

energies. Also in fig. 1, a peak near 5 eV loss is resolved in the 75 eV spectrum but not in the 400 eV spectrum.

Five loss peaks are evident in the first derivative 75 eV LEELS spectrum for pure tin as shown in fig. 1b. The $4d_{3/2}$ loss has an energy of 25.0 ± 0.2 eV and the $4d_{5/2}$ loss occurs at 24.0 ± 0.2 eV (peak 2). These values are very close to the values of $E(4d_{3/2}) = 24.8$ and $E(4d_{5/2}) = 23.8$ reported in ref. [12]. The largest peak in fig. 1b (peak 3) has an energy loss of 13.8 eV and is due to the bulk plasmon excitation in pure tin, in agreement with previous results [4,5]. The surface plasmon (peak 4) has an energy loss of 9.8 eV also in agreement with previous results [4,5]. The weak peak (peak 5) just below the elastic peak has an energy loss of 4.8 eV and has been previously reported [5] and assigned to an interband transition. The energy losses of all five peaks were measured from the energy separation of the steepest negative slope of the derivative spectra because the two plasmon peaks and the interband peak had widths of almost 2.0 eV compared to 0.7 eV for the elastic peak.

Fig. 2 shows the 75 eV LEELS first derivative spectrum from a sputter

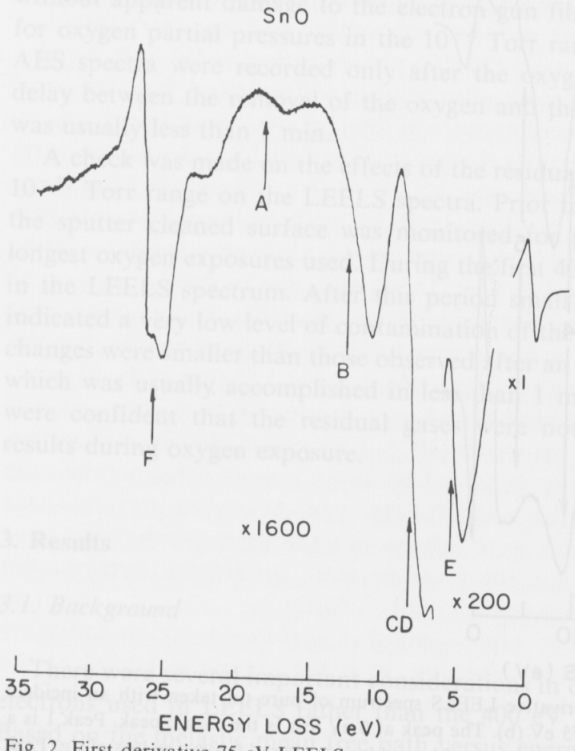

Fig. 2. First derivative 75 eV LEELS spectrum of sputter cleaned SnO powder. Peak A is due to the bulk plasmon of residual SnO_2. Peak B is due to both the surface plasmon of SnO_2 and the bulk plasmon of SnO. Peak CD is discussed in the text. Peak E is an interband transition involving O(2p) initial state. Peak F is the $4d_{3/2,5/2}$ tin ionization loss doublet for oxidized tin.

cleaned bulk sample of SnO powder. Peak A near 18 eV energy loss is the bulk plasmon of SnO_2. Prior to any sputtering this peak was several times larger due to the surface SnO_2 layer on the SnO particles. Its continued presence in the SnO LEELS spectrum is believed due to the failure of the near normal incident ion beam to sputter etch some of the sides of the 10 μm cubic particles of SnO that were exposed to the electron beam. A persistent carbon Auger peak from sputter etched SnO powder lends support to this shadowing effect. Peak B is the bulk plasmon of SnO with an energy loss of 11.6 eV which is close to the value estimated from Powell's [4] data. The sharp peak labeled CD has a loss of 7.9 eV. This peak is a doublet that could only be resolved on oxidized tin substrates but not on SnO or SnO_2 powder samples. The assignment of this peak will be discussed below. The large peak, designated E, has an energy loss of 4.8 eV and is probably due to an O(2p) loss, since it also occurs in the LEELS spectrum of SnO_2. The large peak (F) at about 26 eV loss is the partially resolved $4d_{3/2,5/2}$ tin doublet.

Fig. 3 shows the 75 eV LEELS spectrum of sputtered SnO_2 powder in the form of submicron particles pressed into a solid cake on indium foil. The 4d

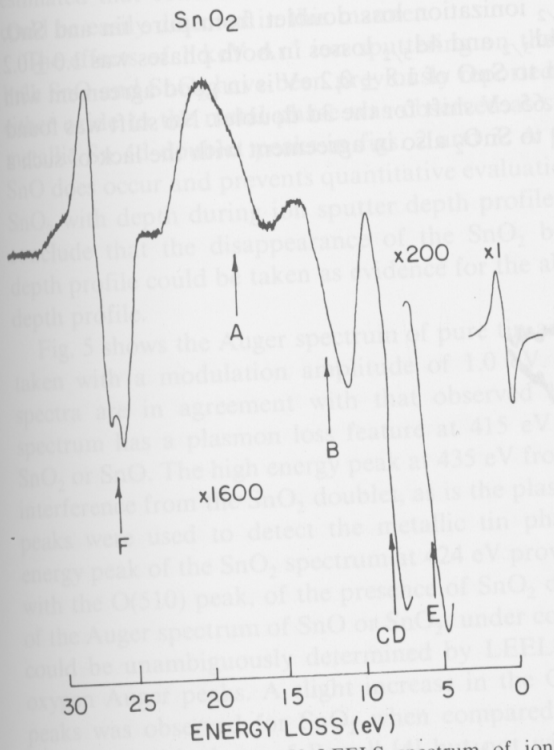

Fig. 3. First derivative 75 eV LEELS spectrum of ion sputtered SnO_2 powder. The peak assignments are the same as those used in fig. 2.

doublet peak (F) occurs at the same energy, within ± 0.15 eV, of that for SnO shown in fig. 2. The bulk plasmon peak, labeled A, occurs at 18 eV energy loss. Prior to any sputter etching it had an intensity about four times that shown in fig. 3. It occurs in an energy loss region relatively free of signals from either SnO or Sn and proved a reliable indicator of the presence of the SnO_2 phase during the oxidation of tin. The bulk plasmon of SnO, labeled B, at 11.6 eV was absent in the unsputtered SnO_2 powder. The decrease of A and increase of peak B form the basis for our previous conclusion [11] that 1 keV Ar^+ ions reduce the surface of SnO_2 to SnO. Peak B has an energy very near to that of the bulk plasmon of SnO (peak B2 in fig. 3 of Powell [4]) and the surface plasmon of SnO_2 (peak C1 in fig. 3 of Powell [4]). Powell did not report numerical values for these peaks in his 400 eV LEELS. Because of the overlap of the bulk plasmon of SnO and the surface plasmon of SnO_2, peak B could not be used to unambiguously identify SnO or SnO_2 during the oxidation of tin except in those circumstances where additional information from peak A or CD was available. Peak CD with a loss energy of 7 eV will be discussed below. As in the case of SnO a large peak, E, occurs at 4.8 eV loss and is assigned to an O(2p) loss.

Fig. 4 shows the $4d_{3/2,5/2}$ ionization loss doublet from pure tin and SnO. The energy splitting of the $4d_{3/2}$ and $4d_{5/2}$ losses in both phases was 1.0 ± 0.2 eV. The energy shift from Sn to SnO of 1.8 ± 0.2 eV is in good agreement with XPS results [2] that show a 1.65 eV shift for the 3d doublet. No shift was found for the 4d doublet from SnO to SnO_2 also in agreement with the lack of such a

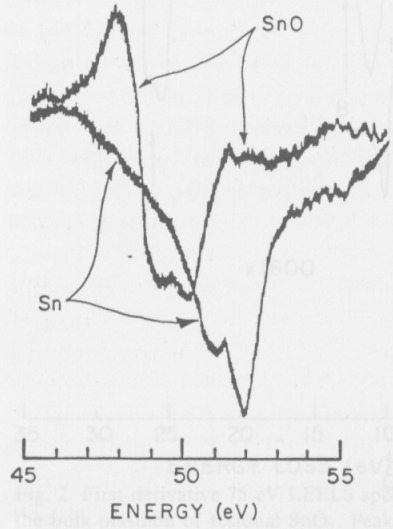

Fig. 4. Ionization loss doublet from $4d_{3/2,5/2}$ tin core levels from pure tin and SnO showing a 1.8 eV shift to lower energy (higher binding energy) for the oxide phase.

shift in the 3d XPS spectra [2]. The intensity of the oxide 4d doublet in either SnO or SnO_2 could therefore be taken as a measure of the total tin bonded to oxygen when either phase is present. Likewise the intensity of the 4d doublet from pure tin represents the contribution of tin bonded to tin. This correlation proved invaluable in unravelling the thickness and chemical stoichiometry of the various oxide films produced during this study.

The relative intensities of the surface plasmon and the 4.8 eV loss peaks in metallic tin were used to monitor the surface purity prior to oxidation. With increasing contamination the Sn surface plasmon intensity decreased while that of the 4.8 eV peak increased due to the loss peaks of SnO and SnO_2 in this region. As the sample was sputter cleaned the ratio of the Sn surface plasmon to that of the 4.8 eV loss peak continually increased until it saturated at the value shown in fig. 1b. Very prolonged ion bombardment with a 3.0 keV, 1000 nA, 1×1 mm^2 ion beam failed to alter this ratio. After such an ion bombardment the O(510) Auger peak was less than 10^{-3} times that of the Sn(435) peak. Thus, we believe the 4.8 eV peak of pure tin shown in fig. 1b is not due to residual oxygen contamination but is likely to be a pure tin interband. It is estimated that contamination coverages of the order of 0.01 of a monolayer could be easily detected in this manner.

The effects of 1 keV Ar^+ ion sputtering on the 75 eV LEELS spectrum of bulk SnO and SnO_2 have been previously reported by us [11]. No reduction of either oxide to the metal phase was observed as shown by the absence of the metallic Sn 4d doublet peaks in figs. 2 and 3. A partial reduction of SnO_2 to SnO does occur and prevents quantitative evaluation of the relative amounts of SnO_2 with depth during ion sputter depth profiles. However, we were able to conclude that the disappearance of the SnO_2 bulk plasmon peak during a depth profile could be taken as evidence for the absence of this phase during a depth profile.

Fig. 5 shows the Auger spectrum of pure tin and bulk sputter cleaned SnO_2 taken with a modulation amplitude of 1.0 eV. The shifts between the two spectra are in agreement with that observed by Powell [4]. The pure tin spectrum has a plasmon loss feature at 415 eV that is not present in either SnO_2 or SnO. The high energy peak at 435 eV from pure tin is relatively free of interference from the SnO_2 doublet, as is the plasmon loss line at 415 eV. Both peaks were used to detect the metallic tin phase after oxidation. The low energy peak of the SnO_2 spectrum at 424 eV proved a reliable indication, along with the O(510) peak, of the presence of SnO_2 or SnO. Careful measurements of the Auger spectrum of SnO or SnO_2, under conditions where the two phases could be unambiguously determined by LEELS, gave no shift in the tin or oxygen Auger peaks. A slight increase in the O(510) peak relative to the Sn peaks was observed for SnO_2 when compared to SnO. These results are in agreement with those of Powell [4] but not with those of Sen et al. [6] and establish that AES cannot be used to distinguish SnO from SnO_2 is a mixed oxide phase.

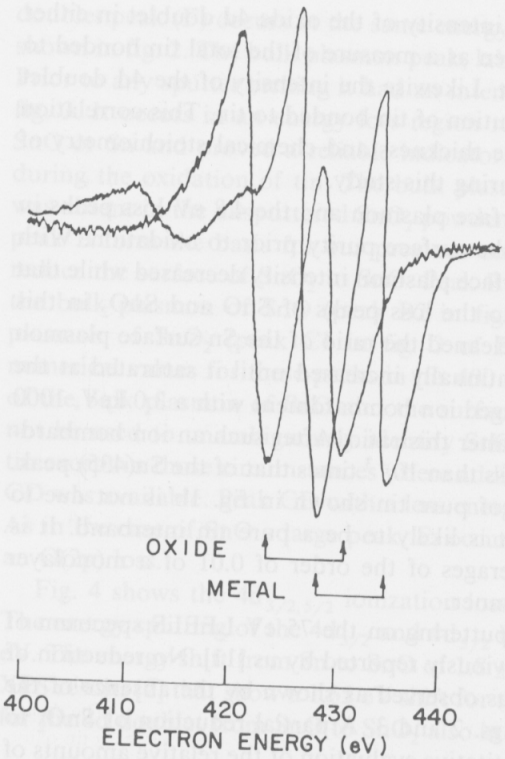

Fig. 5. First derivative Auger spectra of pure tin and SnO_2 showing the shift to lower energy for the oxide spectrum relative to the metallic tin spectrum. The presence of a bulk plasmon loss at 415 eV for the metallic tin spectrum is also shown.

To determine the relative surface sensitivity of 75 eV LEELS and AES three separate polycrystalline tin samples with $\theta_i = 0$, 45, and 60° were sputter cleaned and then simultaneously oxidized at 25°. During the oxygen exposure (10^{-8} Torr region) the LEELS spectrum from the $\theta_1 = 60°$ sample was continuously monitored since this geometry and surface spectroscopy combination was expected to produce the highest surface sensitivity. The oxidation was stopped when the Sn $4d_{5/2}$ peak from metallic Sn had been reduced to a value of about 10% of its maximum value prior to oxidation. The LEELS and AES spectra from each of the three samples is shown in fig. 6. By moving the samples under the fixed electron beam it was determined that the spectra were essentially unchanged from those shown in fig. 6. In particular, the differences in the various spectra at different θ_i were much larger than the differences observed at various places in the same sample. All LEELS spectra, as well as the AES spectra, shown in fig. 6 were taken with the same spectrometer gain.

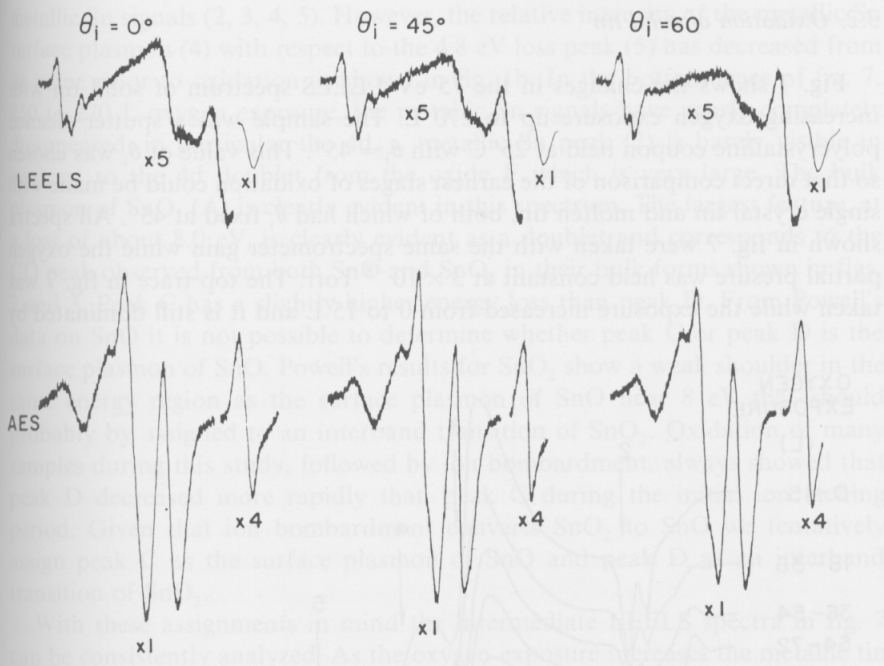

Fig. 6. Auger and LEELS spectra of three polycrystalline tin samples, whose surface normals made angles of $\phi_i = 0$, 45 and 60° to the incident electron beam, after exposure to oxygen. The Auger spectra are dominated by metallic tin signals while the LEELS spectra are dominated by tin oxide signals.

For increasing θ_i in the LEELS spectra the metallic tin $4d_{5/2}$ peak, as well as the metallic tin bulk plasmon, decreases relative to the 4d oxide doublet. The expected increase in surface sensitivity with increasing θ_i is accompanied by increasing tin oxide signals and shows that the oxide layer is on the surface of the sample. At any θ_i the LEELS spectra are dominated by oxide signals, e.g., the largest 4d doublet is that from oxidized tin, while the Auger spectra are dominated by metallic tin signals, e.g., the plasmon loss peak at 415 eV and the main Sn Auger peaks are those from metallic tin. The $\theta_i = 60°$ LEELS spectrum looks very much like that from sputter etched bulk SnO shown in fig. 3. In contrast the $\theta_i = 0°$ Auger spectrum looks very much like that of metallic tin shown in fig. 5. The O(510) intensity for the $\theta_i = 0°$ AES spectrum in fig. 6 is almost one tenth its value observed from bulk SnO_2. These observations illustrate the much improved surface sensitivity of 75 eV LEELS relative to AES.

3.2. Oxidation of solid tin

Fig. 7 shows the changes in the 75 eV LEELS spectrum of solid tin with increasing oxygen exposure up to 270 L. The sample was a sputter cleaned polycrystalline coupon held at 25°C with $\theta_i = 45°$. This value of θ_i was chosen so that direct comparison of the earliest stages of oxidation could be made with single crystal tin and molten tin, both of which had θ_i fixed at 45°. All spectra shown in fig. 7 were taken with the same spectrometer gain while the oxygen partial presure was held constant at 3×10^{-8} Torr. The top trace in fig. 7 was taken while the exposure increased from 0 to 15 L and it is still dominated by

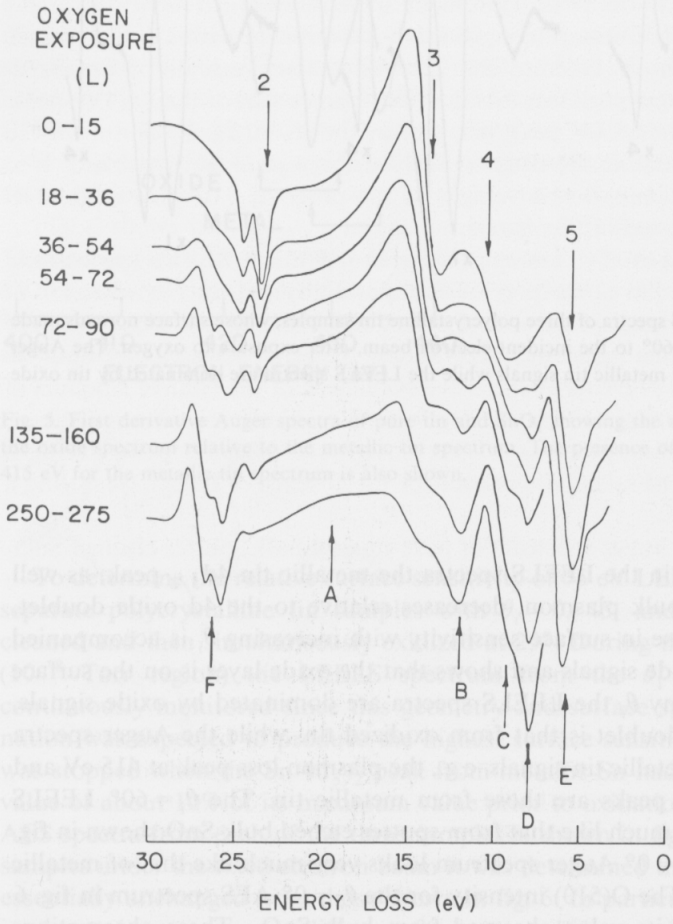

Fig. 7. First derivative 75 eV LEELS spectra taken during early stages of oxygen exposure of a polycrystalline tin sample at 25°C. Peaks A to F have been assigned in fig. 2 and peaks 2 through 4 in fig. 1.

metallic Sn signals (2, 3, 4, 5). However, the relative intensity of the metallic Sn surface plasmon (4) with respect to the 4.8 eV loss peak (5) has decreased from its value prior to oxidation as shown in fig. 1b. In the bottom trace of fig. 7, 250 to 270 L oxygen exposure, the metallic Sn signals have nearly completely disappeared, in particular the $4d_{5/2}$ metallic Sn peak (2) is barely visible in contrast to the 4d doublet from the oxide F which is very large. The bulk plasmon of SnO_2 (A) is clearly evident in this spectrum. The largest feature, at a loss of about 8.0 eV, is clearly evident as a doublet and corresponds to the CD peak observed from both SnO and SnO_2 in their bulk forms shown in figs. 2 and 3. Peak C has a slightly higher energy loss than peak D. From Powell's data on SnO it is not possible to determine whether peak C or peak D is the surface plasmon of SnO. Powell's results for SnO_2 show a weak shoulder in the same energy region as the surface plasmon of SnO near 8 eV that should probably by assigned to an interband transition of SnO_2. Oxidation of many samples during this study, followed by ion bombardment, always showed that peak D decreased more rapidly than peak C during the initial ion etching period. Given that ion bombardment converts SnO_2 to SnO we tentatively assign peak C as the surface plasmon of SnO and peak D as an interband transition of SnO_2.

With these assignments in mind the intermediate LEELS spectra in fig. 7 can be consistently analyzed. As the oxygen exposure increases the metallic tin 4d doublet (2), bulk (3) and surface (4) plasmons all decrease rapidly. There is a corresponding increase in signals due to SnO and SnO_2. The bulk plasmon of SnO_2 (A) starts to appear at exposure levels of about 150 L (see second spectrum from the bottom in fig. 7). The interband peak of SnO_2, peak D, starts to appear after exposures of only 50 L (see second trace from top in fig. 7). Peak B, due to both the surface plasmon of SnO_2 and the bulk plasmon of SnO, also starts to appear at exposure levels of about 50 L (see third trace from top of fig. 7). Because of overlap with the oxide related peaks it is difficult to follow the decay of the metallic tin surface plasmon (4) much below half its original value. It does appear that it simply decreases in intensity rather than shifts in energy. The very rapid increase in the 4.8 eV loss peak (E) with increasing oxygen exposure reflects its high intensity in the SnO and SnO_2 LEELS spectra as shown in figs. 2 and 3.

Fig. 8 plots the changes in the various LEELS signals with oxygen exposure using the same data as shown in fig. 7. The rapid decrease of the loss peaks associated with metallic tin particularly that of the surface plasmon (4) and the corresponding increases in the loss peaks associated with SnO and SnO_2 are both clearly evident in fig. 8. In nearly all cases the intensity of the various peaks was measured from the actual or estimated peak-to-peak height of the derivative spectra shown in fig. 7. The $4d_{3/2}$ component of the oxide doublet (F) and the $4d_{5/2}$ component of metallic tin (2) were used to minimize the effects of overlap of the two sets of 4d doublets. The intensity of the SnO_2 bulk

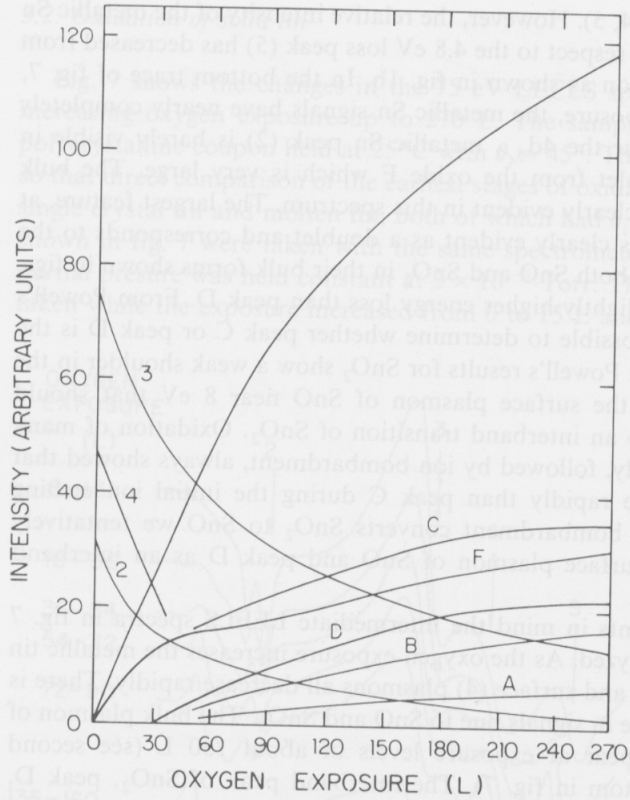

Fig. 8. Decay of metallic tin peaks 2, 3 and 4 and increase of oxidized tin peaks A to F during early stages of the oxidation of polycrystalline tin at 25°C. Because of spectral overlap not all peaks could be determined at exposures below 50 L.

plasmon (A) was estimated from the difference in the spectrum from just above the $4d_{5/2}$ metallic tin peak to a point 20 eV below the elastic peak where the maximum positive value of the SnO_2 bulk plasmon signal occurs. This choice minimized interference with the shoulder of the metallic tin bulk plasmon peak. An extrapolation of the metallic tin surface plasmon peak (4) to zero intensity occurs at an exposure value of 60 L.

To achieve maximum surface sensitivity a polycrystalline tin sample with $\theta_i = 60°$ was oxidized for 40 min at an oxygen partial pressure of 5.0×10^{-8} Torr at 25°C. The decrease in intensity of the metallic tin $4d_{5/2}$ peak with increasing oxygen exposure up to 120 L is given in table 1. The data can be fit to an expression of the form

$$\alpha = -58.7 \ln(R), \tag{1}$$

where α is the oxygen exposure in langmuirs, $R = I(\alpha)/I(0)$, $I(0)$ is the

Table 1
Intensity of $4d_{5/2}$ metallic tin peak as a function of oxygen exposure α (L) using a polycrystalline tin sample at 25°C with $\theta_i = 60°$; the value of $R = I(\alpha)/I(0)$ is also shown

α (L)	$I(\alpha)$	$R(\alpha)$
0	27.0	1.00
15	20.5	0.76
30	15.7	0.58
45	12.5	0.46
60	10.2	0.38
75	7.6	0.28
90	5.7	0.21
120	3.5	0.13

intensity of the $4d_{5/2}$ peak at $\alpha = 0$ and $I(\alpha)$ is the intensity of this peak at α.

The behavior of the LEELS spectra of oxidized polycrystalline tin showed little variation with temperature except for values above 220°C. Measurements were made at 100, 200, 220 and 229°C. The data shown in fig. 7 for 25°C are essentially reproduced when the temperature is held below 220°C. Fig. 9 shows the effects of high temperature oxidation of solid tin using a LEELS depth profile. Two identical oxygen exposures of 3×10^{-8} Torr for 100 min (180 L),

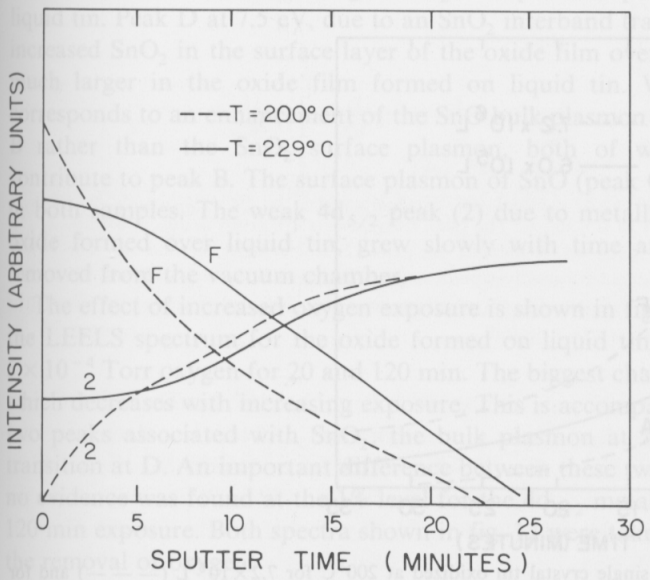

Fig. 9. Depth profile of oxide layers formed on polycrystalline tin at 200°C and 229°C where the $4d_{3/2}$ tin oxide peak (F) and the $4d_{5/2}$ metallic tin peak (2) were continuously monitored.

one at 200°C and one at 229°C, were made on the same polycrystalline sample separated by the removal of the first oxide layer by ion bombardment. After exposure at 229°C the LEELS spectrum clearly showed the presence of the metallic tin $4d_{5/2}$ peak (2) while the identical exposure at 200°C failed to reveal any $4d_{5/2}$ peak from metallic tin. This fact is evident from the intensity of peak (2) at 200°C and 229°C at a sputter time of 0 min in fig. 9. The $4d_{5/2}$ metallic tin peak (2) at 229°C is still about half the value for clean tin produced at the end of the depth profile. The $4d_{3/2}$ oxide peak (F), although lower in value at the surface of the sample oxidized at 229°C, persists at higher values in the interior of the oxide film than it does in the sample oxidized at 200°C. A similar behavior was noted for the O(510) Auger transition taken during an Auger depth profile of these two oxide films (not shown). All of the intensities plotted in fig. 9 were taken with the same spectrometer gain.

The oxidation of single crystal tin at 200°C showed that the oxidation rate, as measured by the decay of the $4d_{5/2}$ metallic tin peak, was five times slower than that observed for polycrystalline tin at 200°C. Data taken from single crystal tin during the early stages of oxidation at 200°C were essentially identical to those shown in fig. 7 for polycrystalline tin at 25°C if the exposure values are multiplied by five.

The oxidation rate of the smooth tin ball at 200°C was very similar to that for single crystal tin at 200°C based on the LEELS spectra taken during the early stages of oxidation.

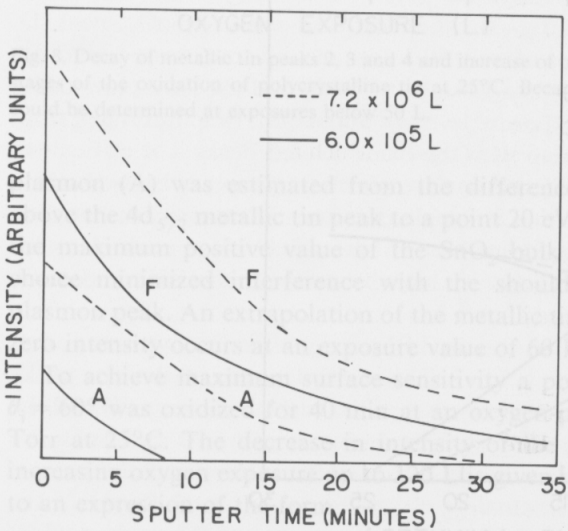

Fig. 10. Depth profile of single crystal tin oxidized at 200°C for 7.2×10^6 L (— — —) and for 6×10^5 L (———) where the intensity of the $4d_{5/2}$ oxidized tin peak (F) and the bulk plasmon peak of SnO_2 (A) were continuously monitored.

A LEELS depth profile of an oxide film grown at 200°C on single crystal tin is shown in fig. 10 for two exposures, one for 7.2×10^6 L and one for 6×10^5 L, both with an oxygen pressure at 5×10^{-4} T. Only the variation of the $4d_{3/2}$ oxide peak (F) and the SnO_2 bulk plasmon (A) peaks are displayed. For the 6×10^5 L exposure, the SnO_2 bulk plasmon (A) disappears after about 8 min of sputter time while the $4d_{3/2}$ oxide peak (F) does not disappear until well beyond 30 min sputter time. At the sputter time where the SnO_2 bulk plasmon (A) disappears, the $4d_{3/2}$ oxide peak (F) is still more than half the value at the surface of the oxide film. Similar behavior is evident for the oxide film formed after 7.2×10^6 L exposure except that the SnO_2 persists to a greater depth so that when it disappears after 30 min, the $4d_{3/2}$ oxide peak has dropped to 18% of its value at the surface of the oxide film. This type behavior was also observed in all LEELS depth profiles taken after oxidation for polycrystalline and smooth ball tin samples.

3.3. Oxidation of liquid tin

Fig. 11 shows the LEELS spectrum from the smooth tin ball taken after a 20 min, 5×10^{-4} Torr (6×10^5 L) oxygen exposure in the solid state ($T = 200$°C) and in the liquid state ($T = 240$°C). The sample was ion etched to clean tin before each exposure. The major difference in these two spectra occurs at energies corresponding to the bulk plasmon of SnO_2 (A) and peak B. The oxide on the solid tin has a much larger SnO_2 bulk plasmon peak than the oxide on liquid tin. Peak D at 7.5 eV, due to an SnO_2 interband transition, confirms the increased SnO_2 in the surface layer of the oxide film over solid tin. Peak B is much larger in the oxide film formed on liquid tin. We believe that this corresponds to an enhancement of the SnO bulk plasmon contribution to peak B rather than the SnO_2 surface plasmon, both of which are known to contribute to peak B. The surface plasmon of SnO (peak C) is nearly the same in both samples. The weak $4d_{5/2}$ peak (2) due to metallic tin, evident in the oxide formed over liquid tin, grew slowly with time after the oxygen was removed from the vacuum chamber.

The effect of increased oxygen exposure is shown in fig. 12 which compares the LEELS spectrum for the oxide formed on liquid tin (240°C) exposed to 5×10^{-4} Torr oxygen for 20 and 120 min. The biggest change occurs in peak B which decreases with increasing exposure. This is accompanied by a rise in the two peaks associated with SnO_2, the bulk plasmon at A and the interband transition at D. An important difference between these two exposures was that no evidence was found at the 1% level for the $4d_{5/2}$ metallic tin peak (2) after 120 min exposure. Both spectra shown in fig. 12 were taken within 3 min after the removal of oxygen.

Fig. 13 shows the ratio of the $4d_{5/2}$ metallic tin peak to that of the $4d_{3/2}$ oxide peak as a function of time after removal of oxygen. The sample had been

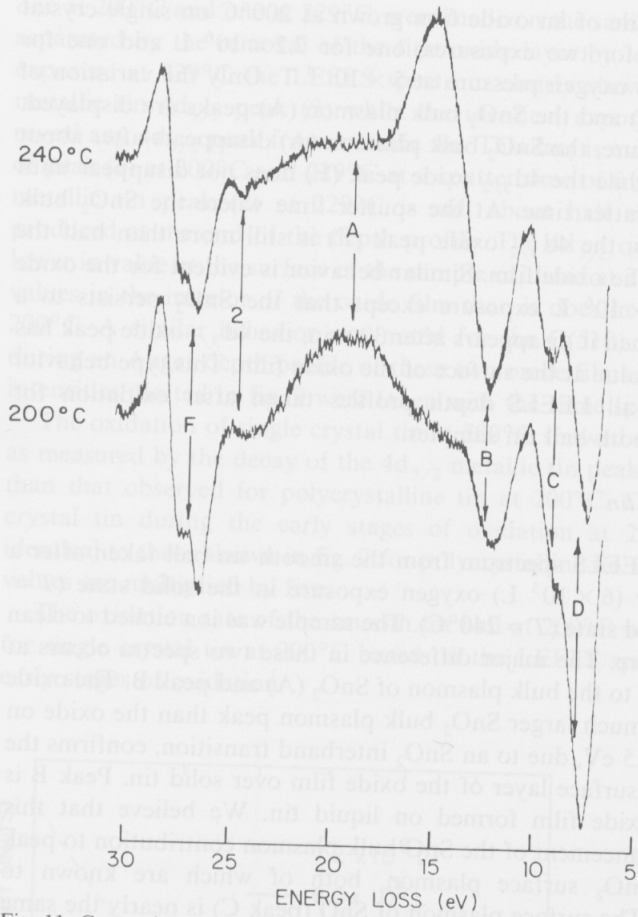

Fig. 11. Comparison of the 75 eV LEELS spectra of solid (200°C) and liquid (240°C) tin after identical oxygen exposures of 6×10^5 L. The peak assignments are given in fig. 2 and fig. 7. The liquid tin spectrum has a weak $4d_{5/2}$ metallic tin peak (2) not evident in solid tin. The largest difference between the two spectra involves peak A (bulk plasmon of SnO_2) and peak B (surface plasmon of SnO_2 and bulk plasmon of SnO) which suggests that the solid oxide formed over liquid tin has less SnO_2 in the near surface region.

exposed at 240°C for 120 min at 5×10^{-4} Torr (3×10^6 L). During the time after oxygen exposure the sample was maintained at 240°C to determine the stability of the oxide layer. For the first 20 min no evidence of the $4d_{5/2}$ metallic tin peak was found above the 1% detection limit, although an Auger spectrum taken during this time still showed evidence of the metallic Sn(435) peak. After 20 min the $4d_{5/2}$ metallic tin peak appeared and grew erratically with several cases where it decreased to very low levels over a period of a few seconds.

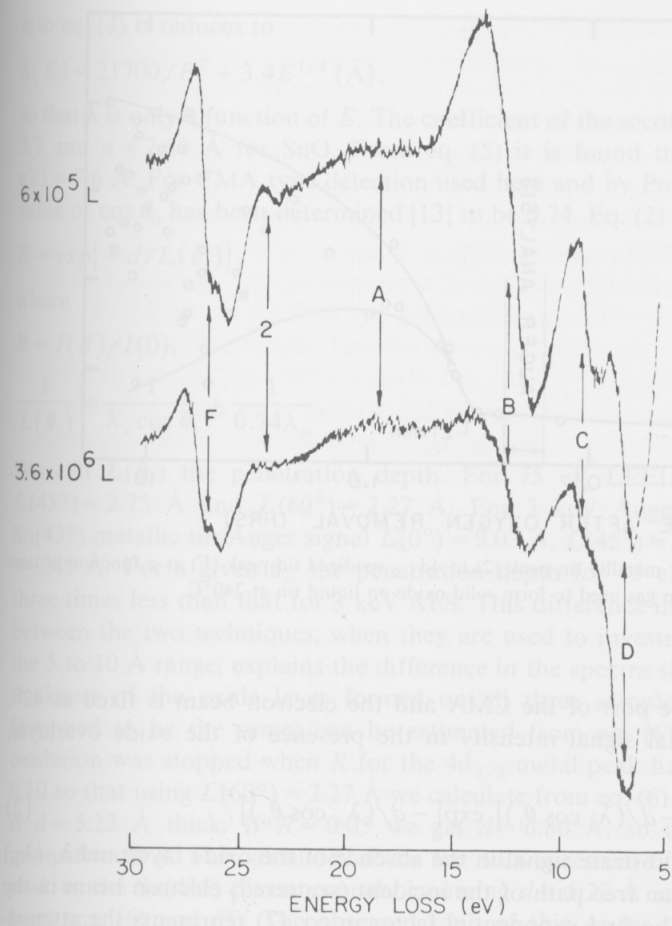

Fig. 12. Comparison of 75 eV LEELS spectra in liquid tin (240°C) after oxygen exposure of 6×10^5 and 3.6×10^6 L.

4. Discussion

4.1. Solid tin

The LEELS and AES spectra shown in fig. 6 for three samples oxidized under identical conditions can be quantitatively understood on the basis of the relative surface sensitivity of the two techniques. Consider a uniform oxide layer of thickness d covering a pure tin substrate. The incident electron beam intersects the sample normal at an angle of θ_i, while the scattered electron beam intersects the sample normal at an angle of θ_o. The angle between the

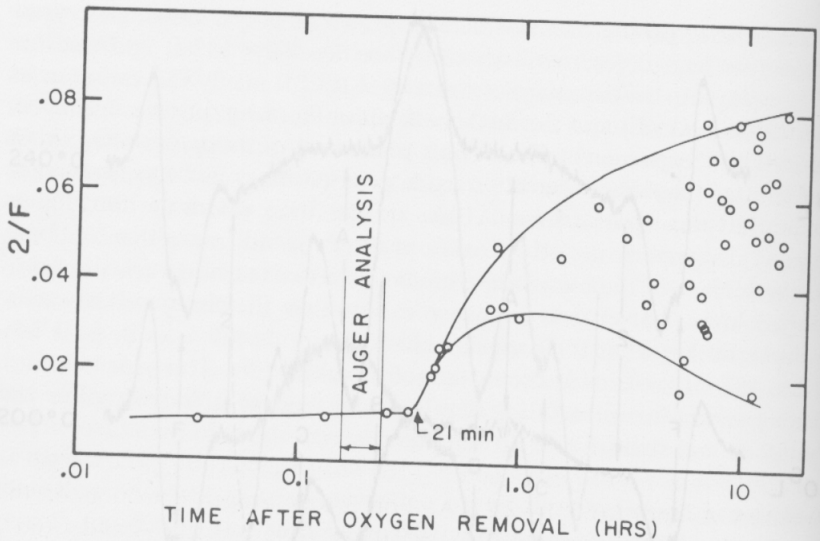

Fig. 13. Ratio of $4d_{5/2}$ metallic tin peak (2) to $4d_{3/2}$ oxidized tin peak (F) as a function of time after removal of oxygen gas used to form solid oxide on liquid tin at 240°C.

annular acceptance port of the CMA and the electron beam is fixed at 42°. The substrate metal signal intensity in the presence of the oxide overlayer, $I(d)$, is given by

$$I(d) = I(0)\exp[-d/(\lambda_i \cos\theta_i)]\exp[-d/(\lambda_o \cos\theta_o)], \tag{2}$$

where $I(0)$ is the substrate signal in the absence of the oxide layer and λ_i (λ_o) is the inelastic mean free path of the incident (scattered) electron beam in the oxide overlayer. The first exponential factor in eq. (2) represents the attenuation of the incident electron beam and the second exponential factor is due to the attenuation of the scattered electron beam. Backscattering corrections have been neglected in eq. (2). The value of λ_i and λ_o were obtained from Seah and Dench [8] for inorganic solids, since our oxide layers consisted of SnO and/or SnO_2. The general expression for λ is

$$\lambda = 2170/E^2 + 0.72(aE)^{1/2}\ (\text{nm}), \tag{3}$$

where E is the electron energy in eV and a is the thickness of an oxide monolayer in nm and is given by

$$a^3 = (A/\rho nN)\times 10^{24}. \tag{4}$$

In eq. (4), A is the molecular weight, ρ is the density in kg/m^3, N is Avagadro's number and n is the number of atoms per molecule. For SnO_2 $\rho = 6950$ kg/m^3, $n = 3$ and $A = 150.7$ so that a is 2.29 Å from eq. (4). Substituting this value of a

into eq. (3) it reduces to

$$\lambda(E) = 21700/E^2 + 3.4E^{1/2}\ (\text{Å}), \tag{5}$$

so that λ is only a function of E. The coefficient of the second term in eq. (5) is 3.7 and $a = 2.59$ Å for SnO. From eq. (5) it is found that for SnO_2, $\lambda(75\ \text{eV}) = 7.6$ Å. For CMA type detection used here and by Powell [4] the average value of $\cos\theta_o$ has been determined [13] to be 0.74. Eq. (2) can be rewritten as

$$R = \exp[-d/L(\theta_i)], \tag{6}$$

where

$$R = I(d)/I(0), \tag{7}$$

$$\frac{1}{L(\theta_i)} = \frac{1}{\lambda_i \cos\theta_i} + \frac{1}{0.74\lambda_o}. \tag{8}$$

We call $L(\theta_i)$ the penetration depth. For 75 eV LEELS $L(0°) = 3.23$ Å, $L(45°) = 2.75$ Å and $L(60°) = 2.27$ Å. For 3 keV Auger detection of the Sn(435) metallic tin Auger signal $L(0°) = 9.03$ Å, $L(45°) = 8.13$ Å and $L(60°) = 7.45$ Å. For a given θ_i, the penetration depth for 75 eV LEELS is about three times less than that for 3 keV AES. This difference in penetration depth between the two techniques, when they are used to investigate oxide films in the 5 to 10 Å range, explains the difference in the spectra shown in fig. 6. The thickness of the oxide layer formed on all three samples shown in fig. 6 (assumed to be the same) can be estimated from eq. (6). For $\theta_i = 60°$ the oxidation was stopped when R for the $4d_{5/2}$ metal peak had been reduced to 0.10 so that using $L(60°) = 2.27$ Å we calculate from eq. (6) that the oxide film is $d = 5.22$ Å thick. If $R = 0.05$ we get $d = 6.80$ Å, so that d is relatively insensitive to R. The calculated R for the AES spectrum of either the Sn(435) peak or the Sn(415) plasmon peak, assuming $d = 5.22$ Å and $\theta_i = 45°$, is 0.53 from eqs. (6) and (7). The observed ratio of this Auger transition was 0.60 which is close to the calculated value. This result shows quantitatively how it is possible for a uniform, metal free oxide layer of approximately 5 Å thickness to produce Auger spectra dominated by metal substrate peaks while the more surface sensitive 75 LEELS signals are dominated by the oxide peaks.

The above analysis assumes that a uniform, metal free oxide layer completely covers the metal substrate over the whole analysis area. Given the nearly monolayer penetration depth for 75 eV LEELS it was desirable to investigate whether it can be used to determine the continuity of thin oxide layers since this is a necessary condition for an oxide film to have adequate strength to suppress Marangoni convection. Let x be the fraction of the surface free of oxide and $1 - x$ be the fraction of the surface covered by a uniform, metal free oxide island of thickness d_1. The intensity of the substrate metal signal is now

$$I(d) = x\, I(0) + (1 - x)\, I(0)\, \exp[-d_1/L], \tag{9}$$

where the first term is due to the oxide free surface and the second term is due to the oxide islands. Solving eq. (9) for R as defined by eq. (7) we obtain

$$R = x + (1 - x)\exp[-d_I/L]. \tag{10}$$

It is instructive to consider the limiting case of eq. (10) when $d_I = \infty$, which represents islands whose thickness is much greater than L. Eq. (10), as expected reduces to $R = x$ for $d_I \gg L$. A more realistic case is when $d_I = 2d$, where d is the thickness calculated from R when the oxide layer is assumed continuous and is given by eq. (6). If $d_I = 2d$ then eq. (10) can be solved for x in terms of R using eq. (6) and one obtains

$$x = R/(1 + R) \quad \text{for} \quad d_I = 2d. \tag{11}$$

If $R = 0.5$ the maximum unoxidized surface fraction is 0.5 for $d_I = \infty$ but only 0.33 for $d_I = 2d$. As R approaches zero the maximum permitted value of x for $d_I = 2d$ approaches that for $d_I = \infty$. If $R = 0.10$ then $x = 0.100$ for $d_I = \infty$ but $x = 0.091$ for $d_I = 2d$. Thus, even for the more realistic case of $d_I = 2d$ less than 10% of the surface can be completely free of oxide if R is 0.10. This analysis of an island oxide model shows that the key requirement to prove high surface coverage of a very thin oxide film is a low value of R. This will insure that the percentage of the oxide covered substrate is high and independent of the assumed thickness of the oxide islands. From eq. (6) low values of R for very thin oxide layers are only possible using techniques with very low penetration depth with respect to the oxide thickness. For 75 LEELS with $L(45°) = 2.75$ Å the value of d required to produce $R = 0.10$ is only 6.33 Å but for 3 keV AES with $L(45°) = 8.31$ Å the oxide must be 19.1 Å to produce an R value of 0.10. Thus for AES, oxide films near 20 Å are required before continuity can be tested while for 75 eV LEELS films near 6 Å can be tested for continuity.

In fig. 8 after about 300 L exposure at 25°C the R value for the $4d_{5/2}$ metallic tin peak (2) is 0.07. To produce this value of R a uniform, metal free oxide layer would have to have a thickness $d = 7.5$ Å, according to eq. (6) with $\theta_i = 45°$. From eq. (10), if $d_I = \infty$ then $x = 0.07$ or if $d_I = 2d = 15.0$ Å then $x = 0.065$. As a result, after 300 L exposure at 25°C tin must have at least 93% of its surface covered by an oxide layer at least 7.5 Å thick to produce $R = 0.07$. We take this result to imply that the surface is essentially continuously covered by a metal free oxide film at all exposures above 300 L for polycrystallize tin at 25°C. Increased oxygen exposure above 300 L reduces R to values near 0.01, the limit of our detection capability, which is consistent with a continuous but thickening oxide film rather than thick islands that fail to cover the last few percent of the metal surface. Because of the similarity in R versus oxygen exposure for polycrystalline tin from 25 to 200°C we extend our assumption of a continuous, metal free oxide layer up to 200°C for oxygen exposures of the order of 300 L. As the temperature approaches the melting

point, e.g., 229°C, the dissolution of oxygen into the metal substrate delays the onset of continuity with exposure. This is illustrated in fig. 9 where $R(200°C)$ for the $4d_{5/2}$ metallic tin peak (2) is less than 0.05 but $R(229°C) = 0.50$. The high value of $R(229°C)$ prevents any conclusions concerning the continuity of the oxide film at 229°C. Single crystal tin was only investigated at 200°C where five times the oxygen exposure was required to produce the same R values for polycrystalline tin at 200°C. We thus expect that oxygen exposures of about 1500 L should be sufficient to produce a continuous, metal free oxide film on single crystal tin. Similar exposure levels are indicated for the smooth tin ball based on the similarity of oxidation rates for this type of sample and single crystal tin. We suspect that the grain size of the tin ball was significantly larger than the 250 μm electron beam size used in the LEELS analysis, so that it would act as essentially a single crystal.

The data shown in table 1 for the oxidation of polycrystalline tin at 25°C suggest a linear growth rate of the oxide film for exposure from zero to 120 L. Assuming uniform oxide layer growth, then from eq. (6) we have $\ln R = -d/L(60°)$ where $L(60°) = 2.27$ Å. Combining this result with eq. (1) for $\ln R$ we get

$$d(\alpha) = 0.039\alpha, \tag{12}$$

so that the growth rate up to 120 L is 0.039 Å per langmuir. From eq. (12) the exposure predicted to form a 2.5 Å thick oxide layer, which is close to the value for one monolayer of either SnO or SnO_2, is 65 L. This is very close to the 60 L value obtained from a linear extrapolation of the metal surface plasmon disappearance in fig. 8. Thus, our results support the hypothesis that for polycrystalline tin a uniform monolayer of tin oxide does occur at oxygen exposure as low as 65 L. For the single crystal tin and smooth tin ball substrates exposures of the order of 300 L should be sufficient to produce a uniform monolayer of oxide.

The simple decrease in intensity, without apparent energy shift, of the surface plasmon (4) of metallic tin (see fig. 7) suggests an island oxide growth during the submonolayer oxide growth regime (< 65 L). During this exposure range the surface plasmon of both Sn and SnO (and perhaps SnO_2 which is interfered with by the SnO bulk plasmon) are simultaneously present. This can only occur if both Sn and SnO phases (and perhaps SnO_2) were present in the top monolayer of the sample i.e., islands of SnO (and perhaps SnO_2) are formed on the metal surface before the oxide layer becomes continuous at a coverage of one monolayer at 65 L exposure level. The surface plasmon results favor the island growth model rather than the random pattern of Sn–O bonding at submonolayer coverage, even though both models are consistent with the exponential decay of the $4d_{5/2}$ metal peak with oxygen exposure up to 100 L (see table 1). It is the spatially extended nature of the surface plasmon that permits this conclusion.

The LEELS and AES depth profiles of a single crystal sample oxidized at 200°C for 20 min and 4 h shown in fig. 10 represent strong evidence for the segregation of SnO_2 in the top portion of the oxide film. The disappearance of the bulk plasmon of SnO_2 (peak A) after a sputtering time of only 8 min compared to the 30 min required to remove all traces of the $4d_{3/2}$ oxide peak (F) suggests that SnO_2 is only present in the upper third of this film. The continued presence of the $4d_{3/2}$ oxide peak (F), which we take to be a measure of the total amount of tin bonded to oxygen as either SnO or SnO_2, can only be explained by the presence of SnO after the disappearance of the SnO_2 bulk plasmon peak. The less rapid decrease in the SnO_2 bulk plasmon signal observed after 4 h oxidation implies that SnO_2 is less surface segregated for this thicker oxide film. The trend of less SnO_2 surface segregation with thicker oxides fits very well with our previous [11] analysis of the native oxide of tin, where, except for a thin surface region, SnO_2 was uniformly distributed throughout the native oxide.

Our model of the oxide formed on solid (polycrystalline) tin as a function of oxygen exposure can now be summarized. For exposures up to 65 L the oxide grows as islands of SnO and perhaps SnO_2 probably a monolayer thick until the entire surface of the metal is covered by the oxide. For higher oxygen exposures both SnO and SnO_2 are clearly present in the thickening oxide layer with the SnO_2 phase enriched at the outer layer of the oxide. The degree of SnO_2 surface segregation is reduced as the oxide becomes thicker, although the surface layer of the native oxide, formed from exposure to laboratory air, is almost completely SnO_2 as we had previously reported [11]. Little change in the composition or continuity of the oxide layer was found from 25 to 220°C. Only at 229°C does the dissolution of oxygen into the metal become evident. Except for a five-fold decrease in growth rate, the oxide formed on single crystal or the large grained tin ball surfaces is essentially the same as for polycrystalline tin. The oxide formed on liquid tin at 240°C is characterized by a larger portion of SnO rather than SnO_2 relative to solid tin. At exposures of the order of 10^7 L a solid oxide, stable for at least 20 min, can be sustained on liquid tin at 240°C.

Our model for the oxidation of solid tin differs from that proposed by Powell [4] in two respects. First let us consider the continuity of oxide layers. Based on the continued presence of metallic tin peaks in his AES and 400 eV LEELS spectra after 5000 L exposure Powell [4] proposed that the oxide contains both metallic tin as well as SnO. From our quantitative analysis of 3 keV AES spectra it is clear that Powell's AES data are consistent with a continuous, metal free oxide layer several monolayer thick since the large penetration depth of AES can produce spectra containing significant metallic tin signals. The penetration depth for 400 eV LEELS at 30° as used by Powell [4] is $L(30°) = 6.22$ Å using $\lambda_i(400) = \lambda_O(400) = 15.6$ Å obtained from eq. (5). This penetration depth is more than twice that of 75 eV LEELS and only

about 70% smaller than that for 3 keV AES. For example, a uniform, metal free oxide layer 14.3 Å thick is required to produce an R value of 0.10 for 400 eV LEELS, compared to 6.33 Å for 75 eV LEELS and 19.1 Å for 3 keV AES. It appears the 400 eV LEELS is not surface sensitive enough to determine the continuity of oxide films in the 5 to 10 Å regime. Just as for 3 keV AES our quantitative analysis of Powell's 400 eV LEELS data reveal it to be consistent with the formation of a continuous, metal free oxide layer at thickness levels up to 10 Å.

The other discrepancy between our model and that of Powell is that be concludes that SnO is the outer oxide. After 5000 L exposure at 25°C, Powell's 400 eV LEELS spectra could be fit by a 3 to 2 ratio of the Sn and SnO spectra respectively. No SnO_2 signals were required. We can estimate the thickness of this oxide layer formed on evaporated tin films from the recent results of Sen et al. [7]. Our samples cannot be used to estimate the thickness of Powell's oxide layer because our observation that polycrystalline tin forms a thicker oxide than single crystal tin prevents us from extrapolating our data to evaporated tin films. Sen et al. [7], assuming that the oxide is continuous, which our data confirm, calculated an oxide thickness of about 4.0 Å on evaporated tin films after 5000 L exposure. Based on our depth profile studies only the top half of this oxide layer contains any SnO_2 and we estimate that only about half of this region contains SnO_2 with the other half being SnO. Thus about one-fourth of the 4 Å oxide is SnO_2. Since 40% of the 400 eV LEELs signal measured by Powell was due to SnO we estimate that SnO_2 was probably present at the 10% level averaged over the sampling depth of 400 eV LEELS. At this level it would have been difficult to detect any SnO_2 using 400 eV LEELS. Thus Powell's 400 eV LEELS data on evaporated tin films is also consistent with our model of the oxide film concerning the content and distribution of SnO_2 in the oxide film on tin. Powell's UPS data of ref. [3] showed both SnO and SnO_2 phases after a 5000 L exposure. We disagree with Powell's assumption that UPS is less surface sensitive than 400 eV LEELS, which is the basis of his conclusion that SnO is the outer oxide. Quantitative estimates of the penetration depth for UPS are difficult to obtain since it is mainly determined by photoelectrons that have energies in the 10 to 20 eV range. It is precisely this region where the inelastic mean free path of electrons is least known experimentally and least understood theoretically. Having already accounted for Powell's AES and 400 eV LEELS data it seems more likely to assume that UPS is more surface sensitive than 400 eV LEELS and thus able to detect the outer SnO_2 layer. We believe that all of our data as well as those of Powell [4] on tin oxide films up to 10 Å thickness can be explained by a continuous, metal free oxide enriched in SnO_2 in the outer layers of the predominantly SnO phase that forms next to the metal substrate.

The mechanism responsible for the five-fold increase in oxidation rate of polycrystalline tin over that of single crystal tin is unknown. Both samples had

been ion etched prior to oxidation. The effect of annealing at 200°C is not known but it may be sufficient to remove some or all of the structural damage produced by the ion bombardment. The existence of surface defects that could act as oxide nucleation sites on polycrystalline samples not present on the surface of single crystal tin could explain the difference in oxidation rate. Alternately, the low oxidation rate of the single crystal tin could simply be a result of anisotropy of oxidation rates for the bct tin crystal structure.

4.2. Liquid tin

The spectra shown in fig. 11 for the same tin sample exposed to the same dose, one as a liquid (240°C) and one as a solid (200°C) show reduced concentration of SnO_2 in the oxide formed on liquid tin compared to its presence in the oxide formed on solid tin. The increased concentration of SnO in the top few monolayers of the oxide formed over liquid tin is probably related to the enhanced mobility of oxygen in the liquid tin phase which reduces the ability of the oxide to sustain an outer crust of SnO_2 when formed over liquid tin. Increased oxygen exposure at 240°C, shown in fig. 12, increases the SnO_2 content of the outer layers of the oxide. This suggests that the diffusion of oxygen across the oxide layer is not fast enough to compete with the increased thickness of the oxide produced at higher oxygen exposures. The expected reduction of SnO_2 to SnO by diffusion after removal of the oxygen gas could not be confirmed because of the phenomenon shown in fig. 13 which we ascribe to the break up of the solid oxide film. With respect to the original purpose of this study the maintenance of a continuous solid oxide on the surface of liquid tin, even if for only 20 min, should be sufficient to determine if this oxide film can suppress Marangoni convection. This work is now in progress.

5. Summary and conclusion

Continuous oxide films, free of metallic tin, can be grown on both solid and liquid tin using oxygen exposures from 100 to 10^7 L depending on the nature of the tin sample and its temperature. Both SnO and SnO_2 phases are present in all oxide films from the very thinnest (~ one monolayer) to those approaching and including the native oxide of tin. The SnO_2 phase tends to be more strongly surface segregated for the thinner oxides on solid tin. This ordering of the two oxide phases is supported by ion beam LEELS depth profiles and has been shown to be consistent with previous AES, UPS and 400 eV LEELS data. As the temperature of solid tin approaches within several degrees of the melting point the diffusion of oxygen into the metal substrate can be observed with characteristic times of the order of tens of minutes. Polycrystalline tin

from 25 to 200°C oxidizes at a rate of 0.039 Å/L for exposures up to 100 L, which is five times faster than that observed for the oxidation of a single crystal of tin. Prior to complete coverage by the oxide film at an average thickness of one monolayer, island oxide growth occurs as evidenced by the simultaneous presence of the surface plasmon of metallic tin and SnO. At about one monolayer coverage the oxide becomes continuous. A continuous, relatively stable oxide film can be formed on liquid tin at 240°C that should permit a test of the hypothesis that such an oxide film may suppress Marangoni convection in liquid tin.

The LEELS technique is a powerful, unique tool in the study of the early stages of gas/solid and gas/liquid interfaces. Powerful, because of its nearly single monolayer surface sensitivity comparable to that reported for ion scattering spectroscopy and photon or electron stimulated desorption spectroscopy. For example, it was demonstrated that for AES, oxide films near 20 Å are required before film continuity can be tested, while for 75 eV LEELS films near 6 Å can be tested for continuity. Unique because in contrast to these other top monolayer sensitive spectroscopies, the physical basis for the generation of surface plasmons is not strictly localized at essentially one atomic site. As a result the use of surface plasmons in LEELS can help distinguish correlated (island) growth from that of random growth during the early states of reaction.

An unanswered but fundamental question with regard to surface plasmon generation involves the minimum size of an island sufficient to produce a surface plasmon of the same energy as an infinitely extended film. We believe an island about 10 Å across may still produce a surface plasmon. The basis for this speculation is that the existence of a surface plasmon requires band-like electron states and calculations of three-dimensional clusters give evidence of band-like states when the central atom is surrounded by occupied nearest and next nearest neighbor sites. The extension to the two-dimensional case for surface plasmons would be of considerable experimental and theoretical interest.

References

[1] T. Farrell, Metal Sci. 10 (1976) 87.
[2] C.L. Lau and G.K. Wertheim, J. Vacuum Sci. Technol. 15 (1978) 622, and references therein.
[3] R.A. Powell and W.E. Spicer, Surface Sci. 55 (1976) 681.
[4] R.A. Powell, Appl. Surface Sci. 2 (1979) 397.
[5] S.M. Barlow, P. Bayat-Mokhtaki and T.E. Gallon, Surface Sci. 83 (1979) 13.
[6] S.K. Sen, S. Sen and C.L. Bauer, Thin Solid Films 82 (1981) 157.
[7] P. Sen, M.S. Hegde and C.N.R. Rao, Appl. Surface Sci. 10 (1982) 63.
[8] M.P. Seah and W.A. Dench, Surface Interface Anal. 1 (1979) 2.
[9] H. Namba, J. Darville and J.M. Filles, Solid State Commun. 34 (1980) 287.

[10] E. Bertel, G. Strasser, F.P. Netzer and J.D. Matthew, Surface Sci., to be published.
[11] A.J. Bevolo, J.D. Verhoeven and M. Noack, J. Vacuum Sci. Technol. 20 (1982) 943.
[12] M. Cardona and L. Ley, Eds., Topics in Applied Physics, Vol. 26 (Springer, New York, 1978) p. 270.
[13] P. Bayat-Mokhtari, S.M. Barlow and T.E. Gallon, Surface Sci. 83 (1979) 131.
[14] M.P. Seah, Surface Sci. 32 (19720 703.